Thermo-Field Dynamics Approach to Photo-induced Electronic Transitions Driven by Incoherent Thermal Radiation

(Article begins on next page)

26 June 2024

Thermo-field Dynamics Approach to Photo-induced Electronic Transitions Driven by Incoherent Thermal Radiation

Maxim F. Gelin[*,†] and Raffaele Borrelli[*,‡]

†*School of Sciences, Hangzhou Dianzi University, Hangzhou 310018, China*
‡*University of Torino, DISAFA, Largo Paolo Braccini 2, I-10095 Grugliasco, Torino, Italy*

E-mail: maxim@hdu.edu.cn; raffaele.borrelli@unito.it

Abstract

The effects of thermal light – matter interaction on the dynamics of photo-induced electronic transitions in molecules are investigated using a novel first principles approach based on the Thermo-Field Dynamics description of both the molecular vibrational modes, and of the radiation field. The developed approach permits numerically accurate simulations of quantum dynamics of electronic/excitonic systems coupled to nuclear and photonic baths kept at different temperatures. The baths can be described by arbitrary spectral densities and can have any system-bath coupling strengths. In agreement with the results obtained previously by less rigorous methods, we show that the excitation process obtained by the continuous interaction with the suddenly turned on thermal radiation field creates a mixed ensemble having a non-negligible component consisting of a superposition of vibronic eigenstates which can sustain coherent oscillations for relatively long times. The results become especially relevant for the dynamics of electronic transitions upon sunlight excitation. Analytical results

based on time-dependent perturbation theory support the numerical simulations and provide a simple interpretation of the time evolution of quantum observables.

1   Introduction

The capability of using sunlight as a source of energy for any kind of human activity is rooted into the understanding of the fundamental mechanisms that trigger its absorption by molecules, and the subsequent transduction into an electrical voltage difference. From a theoretical point of view the fundamental model of exciton-coupled charge transfer is at the basis of the description of such processes, for which reason this model has received a substantial attention in the last few decades.[1–3] Yet, quite often, the preparation of the initial photo-excited state that triggers the entire charge transfer process, is not described in a consistent and comprehensive way. As most of the research has been focused on time-resolved spectro-scopic studies of materials and molecules, the description of the photo-initiated processes has almost always been based on the semiclassical treatment of light-matter interaction where the electric filed is considered as a time-dependent perturbation with a specific envelope, which controls most of the subsequent dynamics of the excited system.[4,5]

While laser spectroscopy has been a key tool in unraveling the role played by the coupled vibrational-electronic motion in molecules,[6,7] it is now widely recognized that the photo-excitation process induced by lasers is very different from that triggered by the light of sun or other types of incoherent light.[8–10] The significance of quantum coherence, meaning the role of superposition of states that keep a constant phase relation throughout the time evolution of a system, has been recently discussed in detail[11,12] yet the specific assessment of its emer-gence in complex molecular systems is not an easy task. The main reason is that the exact quantum electrodynamics (QED) description of the radiation field and of its interaction with matter is simply overwhelming for most theoretical and computational approaches available. Analytical results have been obtained for simplified models[13–16] but even the simplest system

of chemical interest is often out of reach for most numerical methodologies. Indeed, following the general framework of nonlinear femtosecond spectroscopy, it seems to be logical to adopt the description based on perturbation theory in system-field interactions and use nonlinear response function formalism.[4,5] However, thermal fields do not posses any time envelopes restricting the field energy. Hence perturbation expansion breaks down predicting linearly growing in time populations (see, e.g., Refs.[16,17] and Sec. 4.3 of the present work). This simply indicates that any external perturbation of a system with degenerate levels is "strong". To avoid this divergence, one has to introduce certain dissipation/relaxation processes or finite lifetimes of the excited states (see Refs.[16,18–22] for the discussion of linear and nonlinear responses of quantum and (quasi)classical systems). In the context of the present study, it means the following: If we wish to adopt purely microscopic description and avoid introducing phenomenological dissipative or lifetime parameters, perturbative treatment should be avoided. Beyond lowest-order perturbative approach, description of the system interacting with quantum electromagnetic field is commonly based on Lindblad[23] ("quantum optics approach") or Redfield[24] ("chemical physics approach") frameworks, which are based on the so-called Born-Markov approximation. Refs.[25,26] and[27–29] give, respectively, examples of recent applications of the two approaches. Frequently, interaction of the system with thermal light and dissipative environment is collectively described by Redfield or Lindblad equations.[30,31] In more advanced approaches, the system-field interaction is modeled by employing the Born-Markov approach on the top of the non-Markovian treatment of the system dynamics.[32–34] While certainly justifiable in many circumstances these approaches necessarily neglect non-additive effects arising from the interaction of several baths with the same system.[35,36] The Born-Markov assumptions were relaxed in Refs.[37–40] where the system-field interaction was treated with the hierarchical equations of motion (HEOM) method, but the thermal light spectral density was replaced by the (complex) Lorentzian or by the modified (simplified) Planck's spectral density. Very recently, the *ab initio* mixed quantum-classical pulse ensembles (MQC-PE) technique was applied to simulate photophysics of nucleic acids

excited by sunlight.[41] The latter was described by Planck's spectral density and sunlight-molecule coupling was treated in the leading (linear) order in perturbation theory.

On the other hand, the development of tensor-network techniques for the study of quantum dynamics of complex systems[42,43] and of their extension to treat the effect of temperature on the vibrational degrees of freedom,[44–50] has opened the way to the study of very complex model molecular systems interacting with heat reservoirs of any kind as long as an efficient discretization procedure exists that approximates the continuum of the field into a finite number of bosonic modes.[51,52]

Here we tackle the problem of the interaction of molecules with an incoherent light source within a fully consistent Thermo-Field Dynamics (TFD) formalism, and provide numerical simulations based on the Tensor-Trains (TT), (*i.e.* Matrix Product States (MPS)) representation of the vibronic wave-function. We thereby develop the TFD-TT methodology which permits us to perform numerically accurate simulations of the quantum dynamics of an electronic/excitonic system coupled to nuclear and photonic baths kept at different temperatures, described by arbitrary spectral densities, and having any system-bath coupling strengths. Furthermore, the methodology allows us to handle time-dependent Hamiltonians, scrutinize driven system dynamics, and study the effects due to switching on/off interactions of the system with nuclear and photonic modes. We apply this methodology to vibronic excitation problems, showing the role of vibrational-state superpositions induced by thermal light excitation, and pointing out the differences with standard Markovian treatment of light-matter interaction. The dynamical problem is solved using a newly developed integration technique for solving large ordinary differential equation set in TT format that guarantees a solution with a prescribed accuracy.[53,54]

2 Interaction of Molecular Systems with Incoherent Light within Thermo-Field Dynamics Formalism

Let us consider a quantum system, which interacts with a quantized radiation field. The molecular system is described by some, not yet specified, Hamiltonian H_S, the free quantized radiation field is a bosonic reservoir represented by the bath Hamiltonian H_B, and H_{SB} is the system-bath interaction, hence the total Hamiltonian is given by

$$H = H_S + H_B + H_{SB} \tag{1}$$

where

$$H_B = \sum_k \omega_k b_k^\dagger b_k \tag{2}$$

$$H_{SB} = V \sum_m \left(c_m^\dagger + c_m \right) \tag{3}$$

($\hbar = 1$). Here b_k and $b_k^\dagger$ annihilate and create the photonic mode of frequency ω_k, c_m and $c_m^\dagger$ are the annihilation and creation operators in the electronic/excitonic space of the system, V is the bath coupling operator

$$V = \sum_k \gamma_k \left(b_k^\dagger + b_k \right), \tag{4}$$

and the coupling constants γ_k can be determined by discretizing the spectral density $J(\omega)$ of the thermal radiation source (*vide infra*). Following a standard procedure,[24,55] the spectral density $J(\omega)$ can be obtained from the autocorrelation function of the electric field $C^{BB}(t) = \langle E(t)E(0) \rangle$ which can be written in the usual form[56]

$$C^{BB}(t) = L_2(t) + iL_1(t) \tag{5}$$

with (see for example[24,55,57])

$$L_2(t) = \frac{\xi}{\pi} \int_0^\infty \omega^3 f(\omega) \coth\left(\frac{\beta\hbar\omega}{2}\right) \cos(\omega t) \quad iL_1(t) = -\frac{i\xi}{\pi} \int_0^\infty \omega^3 f(\omega) \sin(\omega t) d\omega \qquad (6)$$

where

$$\xi = \frac{\hbar\mu^2}{6\pi^3 c^3 \epsilon_0} \qquad (7)$$

and the factor form function $f(\omega)$ has been introduced.[55,57] This latter function has the fundamental role of avoiding the unphysical divergence deriving from the point dipole approximation applied to high frequency modes of the electric field, and it has the characteristic features of a low-pass filter.[55] The overall effect of this cut-off function is to modify the super-Ohmic spectral density, ω^3, which is characteristic of any thermal radiation source, with an effective spectral density

$$J(\omega) = \omega^3 f(\omega). \qquad (8)$$

The $L_2(t)$ term corresponds to the correlation function of the noise of the reservoir,[58] and has been used several times to define the coherence time of a thermal radiation field.[59–61] Values raging from 0.61 to 1.34 fs have been reported for a correlation time of the thermal source at 5500 K, depending on the definition used in the actual calculation.[60] Therefore, the average value of 1 fs is usually taken as the characteristic coherence time of sunlight. On the other hand, the term $L_1(t)$ provides energy dissipation from the system, and together they guarantee that during the evolution of the system the fluctuation-dissipation theorem is fulfilled.

Here we choose to model the factor form using an exponential cutoff function and take

$$J(\omega) \propto \omega^3 e^{-\omega/\omega_c}. \qquad (9)$$

We point out that in order to properly simulate the effect of a thermal radiation field the cutoff frequency ω_c must be chosen chosen in such a way that it must not alter significantly

the coherence time of $L_2(t)$ (*vide infra*).

The coupling constants γ_k can now be obtained by a discretization of the spectral density as[62]

$$\gamma_k = \sqrt{\frac{2J(\omega_k)}{\pi \rho(\omega_k)}} \tag{10}$$

where we assume that the radiation field has a density of modes $\rho(\omega) \propto J(\omega)/\omega$,[63] and impose the condition that the integral of the density in the sampling interval $[\omega_{\min}, \omega_{\max}]$ is equal to the number N of field modes. Finally, the sampling point ω_k can be obtained by imposing that the integral of the density up to the kth frequency is equal to the number modes k

$$C \int_{\omega_{\min}}^{\omega_k} \rho(\omega) d\omega = k, \tag{11}$$

where C is a proper normalization constant. Eq. (11) can be numerically solved for any value of k.

Up to this point we have not yet defined the system Hamiltonian. Since we are interested in the behaviour of exciton-vibrational transitions under incoherent excitation we take H_S to be of the standard form[5,46]

$$H_S = \sum_{mn} \epsilon_{nm} c_m^\dagger c_n + \sum_{nl} g_{nl}(a_l + a_l^\dagger)c_n c_n^\dagger + \sum_l \Omega_l a_l a_l^\dagger \tag{12}$$

where a_l and $a_l^\dagger$ are the creation and annihilation operators of the lth molecular vibration with frequency Ω_l, g_{nl} are vibronic coupling constants that depend on the specific system under examination, and ϵ_{nm} are the electronic energies ($n = m$) and electronic couplings ($n \neq m$).

In order to consider the effect of temperature on the bosonic reservoirs we can apply the TFD approach in the form developed by Borrelli and Gelin.[44,46,64] Here we give a snapshot description of the method and refer the reader to the original papers for technical and methodological details. The description starts from the Liouville - von Neumann equation for

7

the total system+field density matrix governed by the Hamiltonian H of Eq. (1). Furthermore, it is assumed that the system resides initially in the ground electronic/excitonic state. Transformation of this Liouville - von Neumann equation to the TFD Schödinger equation involves two steps. First, an additional set of so-called *tilde* operators is introduced and the dynamical problem in the Liouville space is embedded into a new Hilbert space that is the tensor product of the original space and of the new *tilde* space. Second, thermal Bogoliubov transformation[65] is applied, which introduces a new, thermal vacuum state for all bosonic degrees of freedom. Owing to that trick, the initial state of the Bogoliubov-transformed TFD Schödinger equation corresponds to the global (electronic/excitonic+bosonic) ground state.

Unlike previously reported TFD models, the molecular system of the present work is in contact with an environment at temperature T_1, which is usually room temperature (298 K), while the heat bath of the radiation field is at temperature T_2, which, in the case of sunlight is around 6000 K. The extension of the TFD formalism to this case can be straightforwardly accomplished by applying two independent thermal Bogoliubov transformations to the two set of bosonic operators $a_l, a_l^\dagger$ and $b_k, b_k^\dagger$ defined as

$$
\begin{aligned}
e^{iG_1} a_l e^{-iG_1} &= a_l \cosh\left(\theta_l^{(1)}\right) + \tilde{a}_l^\dagger \sinh\left(\theta_l^{(1)}\right) \\
e^{iG_2} b_k e^{-iG_2} &= b_k \cosh\left(\theta_k^{(2)}\right) + \tilde{b}_k^\dagger \sinh\left(\theta_k^{(2)}\right)
\end{aligned}
\tag{13}
$$

where

$$
G_1 = -i\sum_l \theta_l^{(1)}\left(a_l\tilde{a}_l - a_l^\dagger\tilde{a}_l^\dagger\right), \quad G_2 = -i\sum_k \theta_k^{(2)}\left(b_k\tilde{b}_k - b_k^\dagger\tilde{b}_k^\dagger\right)
\tag{14}
$$

and

$$
\theta_l^{(1)} = \operatorname{arctanh}\left(e^{-\beta_1 f_l^{(1)}/2}\right), \quad \beta_1 = 1/(kT_1), \quad f_l^{(1)} = \Omega_l,
\tag{15}
$$

$$
\theta_k^{(2)} = \operatorname{arctanh}\left(e^{-\beta_2 f_k^{(2)}/2}\right), \quad \beta_2 = (1/kT_2), \quad f_k^{(2)} = \omega_k.
\tag{16}
$$

Note the tilde operators act solely on the tilde space. Introducing operator of the total

Bogoliubov transformation

$$G = G_1 + G_2 \tag{17}$$

and taking into account that $[G_1, G_2] = 0$, we obtain the Bogoliubov-transformed TFD Hamiltonian which takes the form

$$
\begin{aligned}
\bar{H}_\theta =& e^{iG} H e^{-iG} \\
=& \sum_{nm} \epsilon_{nm} c_n^\dagger c_m + \sum_l \Omega_l \left(a_l^\dagger a_l - \tilde{a}_l^\dagger \tilde{a}_l \right) + \sum_k \omega_k \left(b_k^\dagger b_k - \tilde{b}_k^\dagger \tilde{b}_k \right) \\
& - \sum_{ln} \frac{g_{ln}}{\sqrt{2}} \left\{ \left(a_l + a_l^\dagger \right) \cosh\left(\theta_l^{(1)} \right) + \left(\tilde{a}_l + \tilde{a}_l^\dagger \right) \sinh\left(\theta_l^{(1)} \right) \right\} c_n^\dagger c_n \\
& + \sum_{kn} \frac{\gamma_k}{\sqrt{2}} \left\{ \left(b_k + b_k^\dagger \right) \cosh\left(\theta_k^{(2)} \right) + \left(\tilde{b}_k + \tilde{b}_k^\dagger \right) \sinh\left(\theta_k^{(2)} \right) \right\} (c_n^\dagger + c_n)
\end{aligned} \tag{18}
$$

The above expression for the Hamiltonian of a vibronic system interacting with a thermal light source is the main result of this section. The Hamiltonian is explicitly temperature-dependent, owing to the renormalized electron/exciton vibrational coupling parameters $g_{ln} \cosh(\theta_l^{(1)})$, $g_{ln} \sinh(\theta_l^{(1)})$, and system-field coupling parameters $\gamma_k \cosh(\theta_k^{(2)})$, $\gamma_k \sinh(\theta_k^{(2)})$.

The corresponding TFD Schrödinger equation reads

$$i\frac{\partial}{\partial t} |\psi(t)\rangle = \bar{H}_\theta |\psi(t)\rangle, \quad |\psi(0)\rangle = |g\rangle|\mathbf{0}\rangle \tag{19}$$

where $|g\rangle$ is the ground electronic/excitonic state of the system and $|\mathbf{0}\rangle$ is the joint vacuum state of the molecular vibrations and field bosons. The TFD Schrödinger equation (19) governed by the Hamiltonian of Eq. (18) is fully equivalent to the Liouville - von Neumann equation governed by the Hamiltonian of Eq. (1). Note that the Hamiltonian of Eq. (18) can be explicitly time-dependent. This is essential, *inter alia*, for scrutinizing effects due to switching on/off thermal fields by introducing appropriate field envelops (see works of Dodin et al.[27], Grinev and Brumer[66] for the study of these effects via approximate methods).

Once the coefficients ϵ_{nm}, γ_k, and g_{kn} are determined it is possible to solve the TFD

Schrödinger equation by using the TT approach as described in the next section.

3   Time Evolution of Tensor Trains

The solution of the time-dependent TFD Schrödinger equation (19) requires efficient numerical methods. Since the introduction of the tilde space doubles the number of nuclear degrees of freedom (DoF), and since a thermal environment can be realistically mimicked only using hundreds of DoFs, especially if the temperature is very high, as in the case of a thermal radiation field, it is essential to use a methodology suitable to treat a large number of dynamical variables. Several techniques have been developed which can, at least in principle, overcome what has been termed the *curse of dimensionality*.[67,68] Several methodologies can nowadays be used to accurately describe the quantum dynamics of a system with a large number of DoFs, among which Multi-Configuration Time-Dependent Hartree (MCTDH),[68] Multiple-Davydov's Ansätze (MDA),[69] Hierarchical Equations of Motion (HEOM),[47,54,70] Quasi-Adiabatic Path Integrals (QUAPI)[71] and the wide family of Tensor-Network representations[72,73] are probably the most representative. Here we employ the so-called Tensor Train (TT) format (or Matrix Product States (MPS) in the physics literature) to efficiently represent the vibronic wavefunction. The reader is referred to the original papers[74–77] for a detailed analysis of the TT decomposition and to a recent review for its specific application to TFD formalism.[46]

Several techniques exist to compute the time evolution of TT/MPS.[75,78–82] Recently the time-dependent variational approach (TDVP) has been applied to solve TFD equations in TT format.[44] This method solves the dynamical equations projected onto the manifold of the TT decomposition using a splitting scheme over the TT cores, providing an accurate evolution with fixed TT ranks, and hence prescribed computational costs. However TDVP accuracy must be checked *a posteriori*, by running several calculations with increasing ranks and verifying the convergence of the solution. Furthermore, in certain type of problems TDVP may

not preserve certain invariants of the solution.[47,83] Here we employ a new methodology for TT integration referred to as Time-dependent Alternating Minimal Energy solver (tAMEn), which has already been succesfully applied to large quantum dynamical problems.[53,54] This integration technique automatically adjusts the TT ranks of the solution during the evolution to achieve a prescribed accuracy, and can fulfill the norm conservation law and any other type of *a priori* known linear invariants of the differential equation exactly, provided the state defining the invariant admits an exact TT decomposition. We briefly sketch the basic ideas behind the tAMEn algorithm and leave the reader to the original paper[53] for the mathematical and numerical details.

Firstly, we discretise the state $|\psi(t)\rangle$ in time by introducing a basis of Lagrange polynomials $\{P_\ell(t)\}_{\ell=1}^L$, centered at the Chebyshev points $\{t_\ell\}_{\ell=1}^L \subset [0,T]$. This gives us an approximation

$$|\psi(t)\rangle \approx \sum_{\ell=1}^L \sum_{i_1,\ldots,i_N} C_{t_\ell}(i_1,\ldots,i_N)|i_1\rangle \otimes \cdots |i_N\rangle P_\ell(t), \qquad t \in (0,T], \quad 0 < t_1 < \cdots < t_L = T.$$

(20)

The nodal coefficients $C_{t_\ell}(i_1,\ldots,i_N)$ altogether can be collected into a tensor of order $N+1$, which is approximated by a TT decomposition

$$C_{t_\ell}(i_1,\ldots,i_N) \approx C^{(1)}(i_1)C^{(2)}(i_2)\cdots C^{(N)}(i_N) \cdot C^{(N+1)}(\ell).$$

(21)

where $C^{(k)}(i_k)$ is a $r_{k-1} \times r_k$ complex matrix, $k = 1,\ldots,N$, and $C^{(N+1)}$ stores the index associated with the time points t_ℓ.

In turn, the time derivative in (19) can be cast onto the polynomials $P_\ell(t)$, resulting in the *differentiation matrix* with elements $D_{\ell,\ell'} = \frac{dP_{\ell'}}{dt}(t_\ell)$, $\ell, \ell' = 1,\ldots,L$, which can be computed explicitly. Turning D into a super-operator $\hat{D} = D \otimes I$ (where I is the identity operator matching the size of $|\rho\rangle$), the differential equation (19) is approximated by an algebraic

equation

$$\hat{A}|\boldsymbol{\psi}\rangle = |\boldsymbol{b}\rangle, \qquad \text{where} \tag{22}$$

$$\hat{A} = \hat{D} + i\hat{H}_A ,$$

$$|\boldsymbol{b}\rangle = (D1_L) \otimes |\psi(0)\rangle,$$

and 1_L is a vector of ones of size L. Having solved this equation, we can interpolate $|\boldsymbol{\psi}\rangle$ at any sought time $t \in [0, T]$. The method is implemented by checking the convergence of this approximation using the pseudospectral approximation theory,[84] together with an adaptive selection of the step size T or degree L.[53]

The algebraic equation (22) can be solved using the Alternating Minimal Energy (AMEn) method,[85] which builds upon the Alternating Linear Scheme (ALS).[86] A TT decomposition (21) can be rewritten as a subspace reduction problem by stretching the kth TT core into a vector $|c^{(k)}\rangle \in \mathbb{R}^{r_{k-1}p_k r_k}$ with elements

$$|c^{(k)}\rangle(\alpha_{k-1}i_k\alpha_k) = C^{(k)}_{\alpha_{k-1},\alpha_k}(i_k), \tag{23}$$

and by introducing the *frame* operator $\hat{C}_{\neq k} \in \mathbb{R}^{(p_1 \cdots p_N L) \times (r_{k-1}p_k r_k)}$ such that $\hat{C}_{\neq k}|c^{(k)}\rangle$ contains all elements $C_{t_\ell}(i_1, \ldots, i_N)$ (for uniformity of notation, we can let $p_{N+1} = L$). A tedious but straightforward calculation shows that $\hat{C}_{\neq k}$ is constructed from all but kth TT cores.[86] Crucially, if both $\hat{A}$ and C are represented in the TT format, the computation and solution of the Galerkin reduced system

$$\langle\hat{C}_{\neq k}|\hat{A}|\hat{C}_{\neq k}\rangle \cdot |c^{(k)}\rangle = \langle\hat{C}_{\neq k}|\boldsymbol{b}\rangle \tag{24}$$

is cheap, requiring at most $\mathcal{O}(Np^2r^3)$ operations. The ALS algorithm seeks a TT approximation to the solution of Eq. (22) by iterating over $k = 1, \ldots, N + 1$, solving Eq. (24) in each step, and updating the kth TT core $C^{(k)}$ with the elements of $|c^{(k)}\rangle$.

12

The AMEn method[85] empowers ALS with adaptive TT ranks and faster convergence by additionally expanding $C^{(k)}$ by a TT core of the TT approximation of the residual

$$(|\boldsymbol{b}\rangle - \hat{A}|\boldsymbol{\psi}\rangle)(i_1, \ldots, i_N, \ell) \approx C^{(1)}(i_1) \cdots C^{(k-1)}(i_{k-1}) Z^{(k)}(i_k) Z^{(k+1)}(i_{k+1}) \cdots Z^{(N+1)}(\ell), \quad (25)$$

where $\left|z^{(k)}\right\rangle = \langle\hat{Z}_{\neq k}||\boldsymbol{b}\rangle - \hat{A}|\boldsymbol{\rho}\rangle\rangle$ can be computed by the secondary ALS iteration similar to Eq. (24). After Eq. (24) is solved, we replace a pair of TT cores with their padded versions,

$$C^{(k)}(i_k) := \begin{bmatrix} C^{(k)}(i_k) & Z^{(k)}(i_k) \end{bmatrix}, \qquad C^{(k+1)}(i_{k+1}) := \begin{bmatrix} C^{(k+1)}(i_{k+1}) \\ 0 \end{bmatrix}. \quad (26)$$

The zeros in $C^{(k+1)}$ preserve the whole tensor C (and hence the state $|\psi\rangle$ remains correct), but the extra terms in $C^{(k)}$ enrich the frame operator $\hat{C}_{\neq k+1}$ for the next iteration, and the global residual information supplied by $Z^{(k)}$ accelerates the convergence towards the true solution of Eq. (22). Before the expansion (26), we can also truncate the TT rank r_k by computing a truncated Singular Value Decomposition (SVD) of $C^{(k)}$.[74] The combination of this truncation and expansion (26) allows the tAMEn algorithm to adapt TT ranks according to the desired error threshold.

Numerical experiments demonstrate that the error fluctuates within a constant interval for long periods of time.

4 Vibronic excitations by incoherent light sources

We begin with a brief description of technical details of the simulations used in the present work. The proper choice of the sampling interval $[\omega_{\min}, \omega_{\max}]$ in the discretization of the spectral density of the thermal field via Eq. (11) is crucial for the convergence of the numerical simulations and depends on the cutoff frequency. We chose the interval as $[\omega_c/10, 2\omega_c]$ with $\omega_c = 2.0$ eV, and discretize the field by using $N = 200$ modes. This ensures that the

coherence time of the filed is about 2 fs, which is very close to the coherence time of the radiation produced by a black-body source. After the introduction of the *tilde* space for the thermal field, we have a total of $2N = 400$ field DoFs treated at a full quantum mechanical level at finite temperature. If s is the number of the system DoFs, the total number of the simulated DoFs is $s + 2N$.

The structure of the TT used for the numerical simulations is schematically described as

$$\underbrace{C\left(i_1\right)\cdots C\left(i_s\right)}_{\text{system}}\underbrace{C\left(i_{s+1}\right)\cdots C\left(i_{s+2N}\right)}_{\text{radiation}}. \tag{27}$$

where each DoFs is associated with a core of the TT representation. In our simulations, we use a six-point Chebyshev discretization of the time-derivative operator with a maximum time step of 0.5 fs, and set a global error threshold of 10^{-4}. However we recall that the algorithm is both time and rank adaptive.

4.1   Franck-Condon Harmonic excitation

Let us now focus on a specific system consisting of two electronic states, and one high frequency molecular vibration having a strong Franck-Condon activity, that interacts with a thermal radiation field at 6000 K. We refer to this as the Harmonic-Oscillator Franck-Condon (HOFC) model. More specfically we consider an oscillator with frequency $\Omega = 1400$ cm^{-1} and reorganization energy $\lambda = 514$ cm^{-1} corresponding to a linear vibronic coupling $g = 1200$ cm^{-1}, which are typical values for organic dyes with vinyl stretching vibrations with a strong Franck-Condon activity.[2,87,88] We point out that, to the best of our knowledge, this is the first numerical calculations of this rather simple model based on the Hamiltonian described in Sec. 2 which takes into account the effect of two heat sources on a molecular system.

In figure 1 we report the dynamics of the electronic populations during the excitation process. It is readily seen that, in agreement with the standard picture of Einstein theory,[24] a

steady increase in the population of the excited state is observed. We point out that the rate of the population rise depends on the strength of the interaction with the electromagnetic field, and that under standard sunlight conditions it can be of the order of nanoseconds or smaller. Since simulations for such long times are prohibitive we consider a stronger system-field interaction providing excitation rates of the order of a few hundreds of femtoseconds. While this is an arbitrary choice, we will show that several properties of the system are independent of the strength of interaction as long as this remains relatively weak. In addition, if the system-field interaction can be adequately described by the lowest-order perturbation theory (see Sec. 4.3 for the discussion of this issue), a specific value of the system-field coupling can be merely considered as a scaling factor. We further notice that the stationary values of the populations of the electronic states fulfill the detailed balance principle.

Let us now turn our attention to the physical behaviour of the HOFC model under the effect of the thermal radiation field. Figure 2 shows the average values of the occupation number of the excited electronic state and of the position of the oscillator as a function of time. Both increase with time and show an oscillatory behaviour with a period of about 24 fs, which is clearly associated to the frequency of the harmonic oscillator. We notice that, albeit the oscillations are of relatively small amplitude, they last for quite a long time.

A better insight into the dynamics of the oscillator can be gained by looking at the average position of the oscillator projected onto the excited state and normalized by the overall electronic population, which removes the component of the position associated to the population of the ground electronic state. This observable is reported in figure 3. It is readily seen that the oscillator swiftly moves from 0 to the almost -1 and keeps on oscillating around the value -0.76 which corresponds to the dimensionless displacement of the Franck-Condon mode, which is given by $d = g/\Omega$. The oscillations are small, and are almost independent of the strength of the system-bath coupling, which means that they are an inherent property of the system that is triggered by the interaction with field.

It is worth noticing that these oscillations can only be generated by a *coherent superposi-*
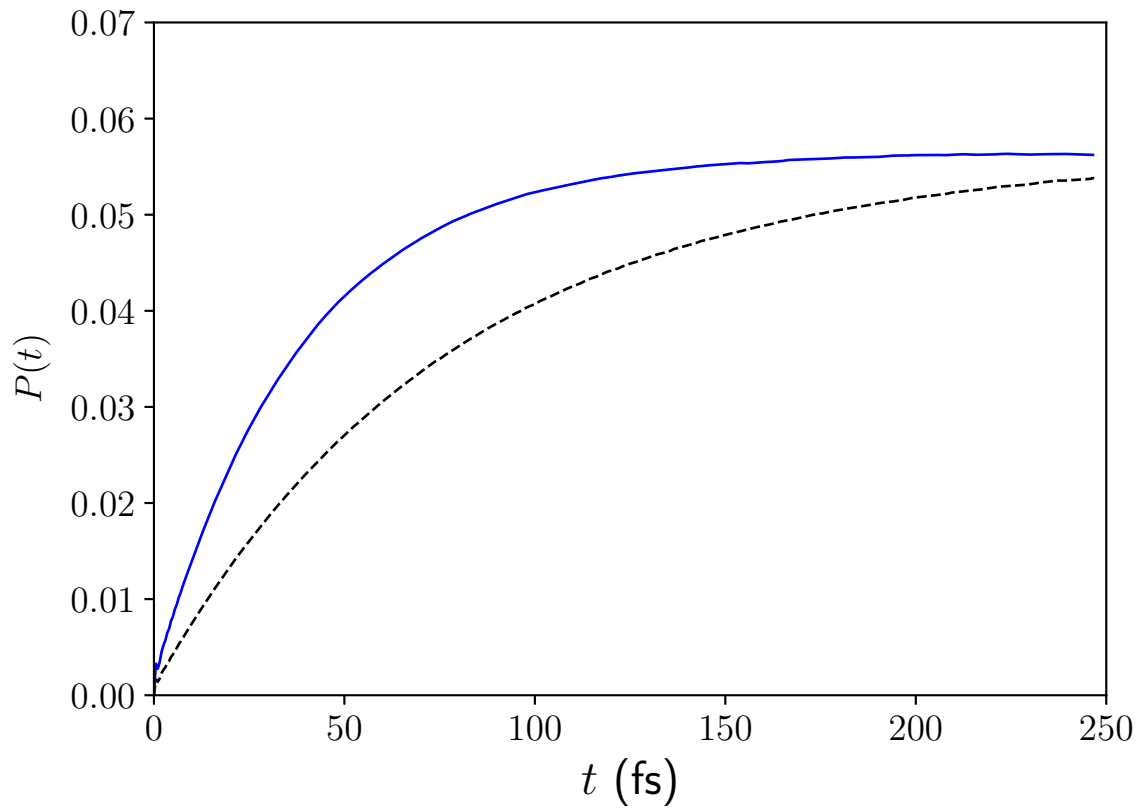
Figure 1: Population of the electronic excited state of the HOFC model as a function of time; blue line $\lambda = 40$ cm^{-1}, dashed line $\lambda = 20$ cm^{-1}
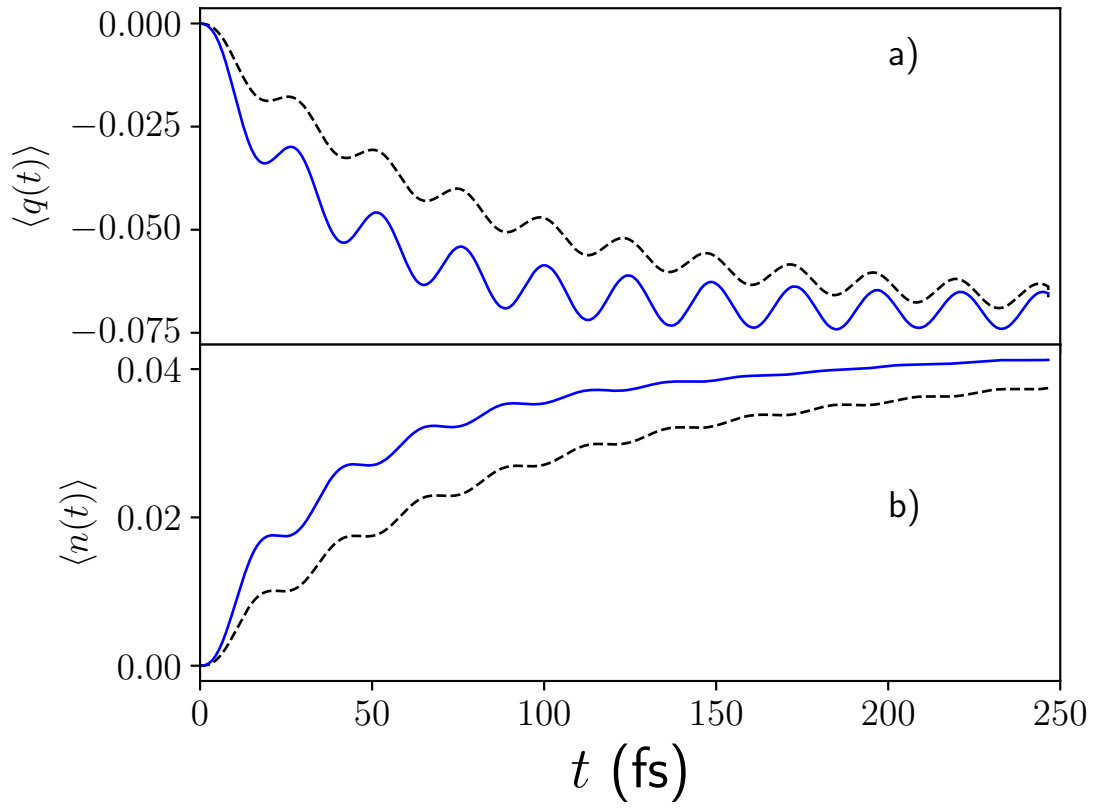
Figure 2: a) Average position of the oscillator in the HOFC model normalized by the electronic population and b) occupation number of the electronic excited state as a function of time; blue line $\lambda = 40$ cm^{-1}, dash line $\lambda = 20$ cm^{-1}.
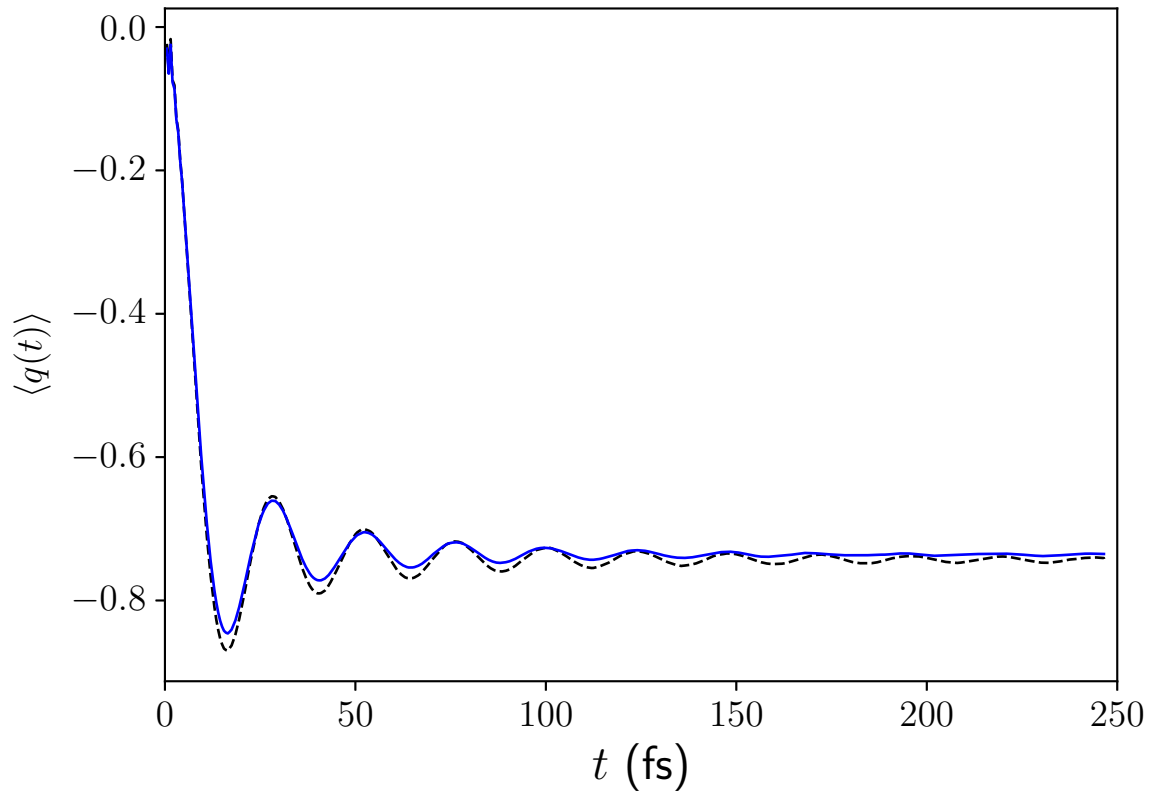
Figure 3: Average position of the oscillator in the electronic excited state of the HOFC model as a function of time; blue line $\lambda = 40$ cm^{-1}, dashed line $\lambda = 20$ cm^{-1}.

tion of harmonic oscillator states in the excited electronic state. We thus show by numerically accurate *ab initio* simulations that the suddenly turned on thermal radiation creates an excited state density matrix that is a not a statistical mixture but retains a small component of a pure state for a relatively long time – the result which was demonstrated on several model systems by applying various approximate methods (see Ref.[89] for a recent review).

It should be noted that all calculations of the present section are based on the TFD Schrödinger equation (19) which assumes instantaneous switching-on of the thermal field at time $t = 0$. Electronic coherences produced by switching on/off thermal fields behave differently. If the switching on/off times are comparable with the characteristic system dynamics timescales, then the coherences, after the transient time, become time-independent (stationary), and their absolute values match those of coherences produced by instantaneous excitation.[66] It will be interesting to scrutinize this result (obtained within perturbation theory in system-field interaction) against numerically accurate TFD-TT simulations. In contrast, coherences induced by a slow (in comparison with the intrinsic system dynamics) switching on/off thermal fields were shown to be negligible in comparison with populations.[27,89]

4.2 Franck-Condon Harmonic Excitation in Molecular Aggregates

As shown in the previous section an incoherent thermal radiation field can generate a small coherent superposition of eigenstates, which gives rise to an oscillatory behaviour in the population, and in the position observables. The question now arises whether this behaviour can be observed in more complex systems such as molecular aggregates. This aspect is of crucial importance when we consider that aggregation phenomena on semiconductor surfaces can severely limit the efficiency of opto-electronic devices; hence shedding light on the states prepared by an incoherent radiation is fundamental for harnessing solar energy.[90,91]

In order to tackle this question we consider the excitation of a molecular dimer in which each monomer has a high frequency vibrational mode, and the excited states of the two

units are electronically coupled. The parameters of molecular units are the same as in the preceding model, and the electronic coupling between the two excited states is set to $\epsilon_{23} = 400$ cm^{-1}, which is a typical value for dye aggregates.[92,93]

A detailed understanding of the excitation process of the system can be obtained by looking at the components of the reduced electronic density matrix $\rho_S(t)_{ij}$ shown in figure 4 ($i, j = 2, 3$ refer to the singly-excited electronic states of the dimer). Fig. 4a) shows that the
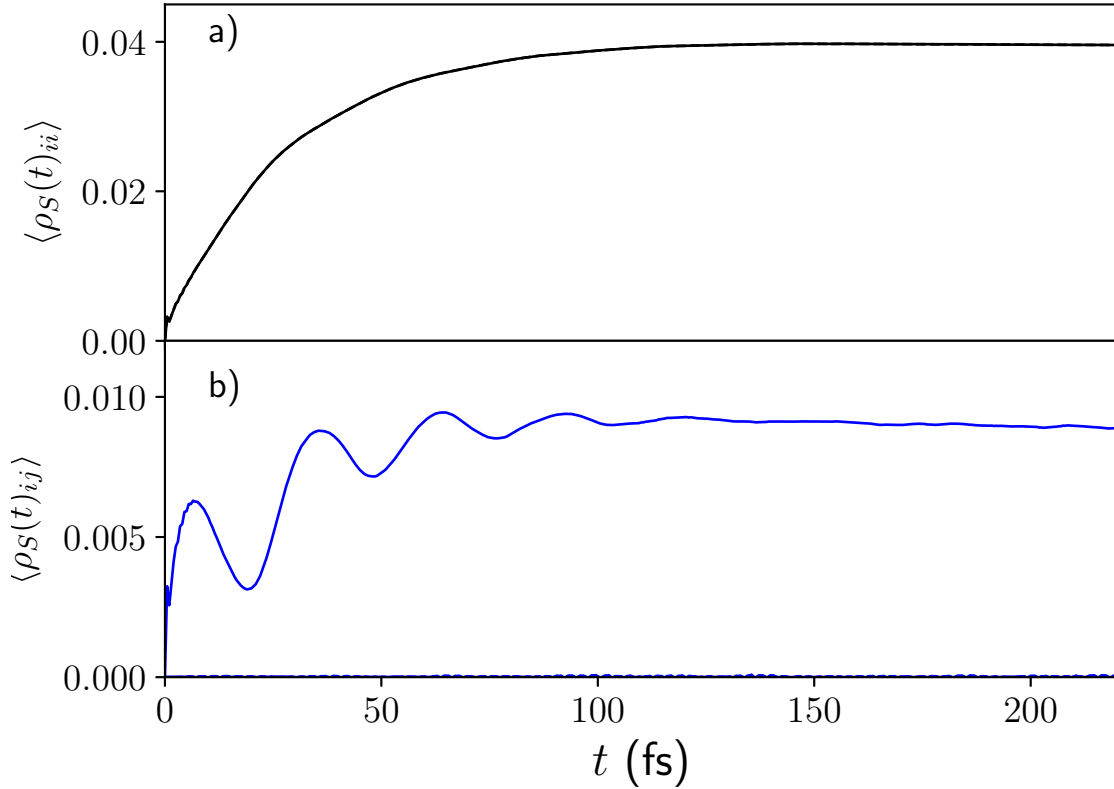

Figure 4: Reduced density matrix of the electronic subsystem of the dimer model. a) diagonal terms, b) real part of the off-diagonal terms. The system-bath coupling is $\lambda = 40$ cm^{-1}. We omit the population of the ground state to improve the clarity of the figure. See the main text for a detailed explanation.

electronic populations of the excited states increase with time and reach a stationary value that satisfies the detailed balance principle. We notice that since the two monomers are equivalent the two populations of 4a) overlap. The real and the imaginary component of the

off-diagonal terms of the reduced density matrix are shown in figure 4b). In this case only the real part of the ρ_{23} term, describing the coherence between the two excited electronic states, is relatively large and shows a characteristic oscillatory behaviour with a period that matches very closely the vibrational period of the high frequency mode of the monomer. All the other components are negligible (around 10^{-6}) and barely visible at the bottom of figure. These oscillations are also observable in the average occupation number and in the average position of the vibrational modes of the two units, as shown in figure 5. In all cases the oscillations decay in a few hundreds of femtoseconds, and the observables reach their steady state values.

As in the preceding model, this behaviour suggests that a transient coherent superposition of vibronic eigenstates is created due to the Franck-Condon type excitation of the ground state wave function driven by the high frequency thermal radiation.

Summarizing: As can be seen from the amplitudes of oscillations in figures 1-5, the coherent component represents only a minor fraction of the overall reduced density matrix, while the statistical mixture is the major component. Yet, the figures clearly show that even a completely incoherent realistically-described photo-excitation induced by the thermal light can sustain coherent motion in the excited electronic states. This result may be considered as not so surprising if we treat the system-field interaction approximately (e. g., in the single photonic mode approximation). However, occurrence of oscillating coherences in the system interacting with thermal field possessing a (quasi)continuum spectrum of photonic modes is much less expected.

4.3 Analytical results

A clearer understanding of the results of our numerical simulations can be obtained by solving the dynamical problem within the second order time-dependent perturbation theory framework. Similar approach was repeatedly used by Brumer and his coworkers,[8,9,16,17,94] but we believe that our presentation here gives a (slightly) different view of the problem and
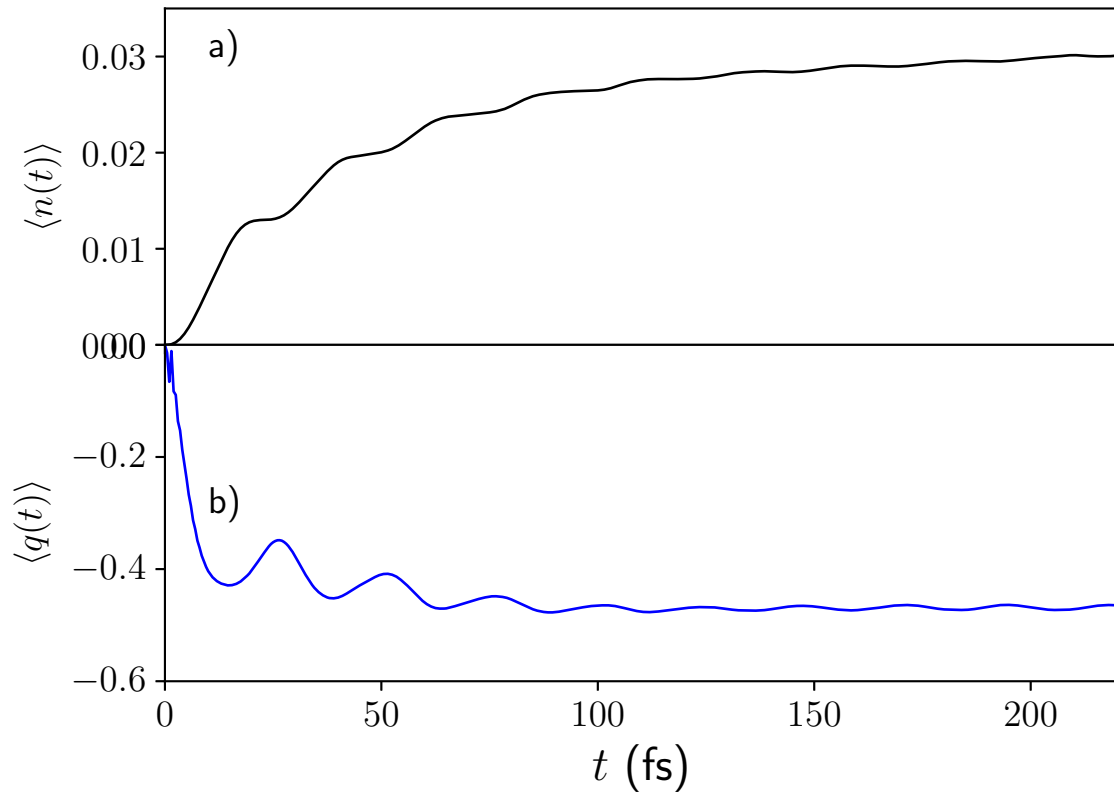
Figure 5: Average occupation number a) and displacement b) of the dimer model projected onto the excited states. The system-bath coupling is $\lambda = 40$ cm^{-1}.

will be helpful for the reader.

Let us consider the system Hamiltonian H_S of Eq. (12) and retain contributions of the ground g and singly-excited e excitonic manifolds only, $H_S = H_g + H_e$. Then we adopt the eigenfunction representation $H_g = \sum_a e_a |a\rangle\langle a|$ and $H_e = \sum_\alpha (\varepsilon_\alpha - i\nu)|\alpha\rangle\langle\alpha|$ where e_a and ε_α are the eigenenergies, $\omega_{\alpha\beta} = \varepsilon_\alpha - \varepsilon_\beta$ and $\omega_{\alpha a} = \varepsilon_\alpha - e_a$ are the transition frequencies, and ν^{-1} is the excited-state lifetime which ensures convergence of perturbation series and makes this treatment phenomenological. ν can be interpreted either as a technical parameter which is introduced for regularization of the time integrals and has to be sent to zero in the end of calculations or as a true physical lifetime parameter. Both options are considered below.

Following Appendix, the (reduced) system density matrix in the singly-excited excitonic manifold can be evaluated in second order of perturbation theory and in the rotating wave approximation in the system-field interaction as

$$\rho^e_{\beta\alpha}(t) = \sum_a \int d\omega J(\omega) n(\omega) G^a_{\beta\alpha}(\omega, t) \tag{28}$$

where

$$G^a_{\beta\alpha}(\omega, t) = G^a_{\beta\alpha}(\omega) \left(e^{-(2\nu + i\omega_{\beta\alpha})t} + 1 - e^{-\nu t} \left[e^{-i(\omega - \omega_{\alpha a})t} + e^{i(\omega - \omega_{\beta a})t} \right] \right) \tag{29}$$

and $G^a_{\beta\alpha}(\omega)$ is defined by Eq. (51). We will refer to the three components in parenthesis as the contributions to coherences (CTC) of the density matrix.

In full agreement with the numerical simulations of Secs. 4.1 and 4.2, Eqs. (28) and (29) show that the thermal light induced density matrix $\rho^e_{\beta\alpha}(t)$ consists of the oscillatory transient contributions (which are proportional to the first and the third terms in Eq. (29)) and a stationary contribution (which is proportional to the second term in Eq. (29)). Eqs. (28) and (29) also clearly demonstrate that $\rho^e_{\beta\alpha}(t)$ is determined by the values of spectral density $J(\omega)n(\omega)$ at all relevant transition frequencies corresponding to $\omega = \omega_{\alpha a}$. Hence the simulations based on Lindblad or Redfield equations (in which the spectral density is frequently taken at a single specific frequency) or on HEOM with Lorentzian spectral density

may become insufficient for faithful evaluation of thermal light induced effects.

The diagonal terms of the density matrix, *i.e.* populations $(\beta = \alpha)$, are determined by the expression

$$G^a_{\alpha\alpha}(\omega) = \frac{\sigma^a_{\alpha\alpha}}{\nu^2 + (\omega - \omega_{\alpha a})^2} \tag{30}$$

and $\rho^e_{\alpha\alpha}(t)$ diverges in the limit $\nu \to 0$ (symbolically, $(\nu^2 + x^2)^{-1} \to \nu^{-1}\delta(x)$). This is not surprising, because perturbation theory breaks down in the case of resonant system-field interaction $(\omega = \omega_{\alpha a})$ which always contributes in the present case. If we keep ν fixed and consider the steady-state limit $t \to \infty$, we obtain

$$\rho^e_{\alpha\alpha}(\infty) = \sum_a \int d\omega J(\omega) n(\omega) \frac{\sigma^a_{\alpha\alpha}}{\nu^2 + (\omega - \omega_{\alpha a})^2}. \tag{31}$$

This expression has clear physical meaning, because $\sum_{a\alpha} G^a_{\alpha\alpha}(\omega)$ is the linear-absorption spectrum at frequency ω.
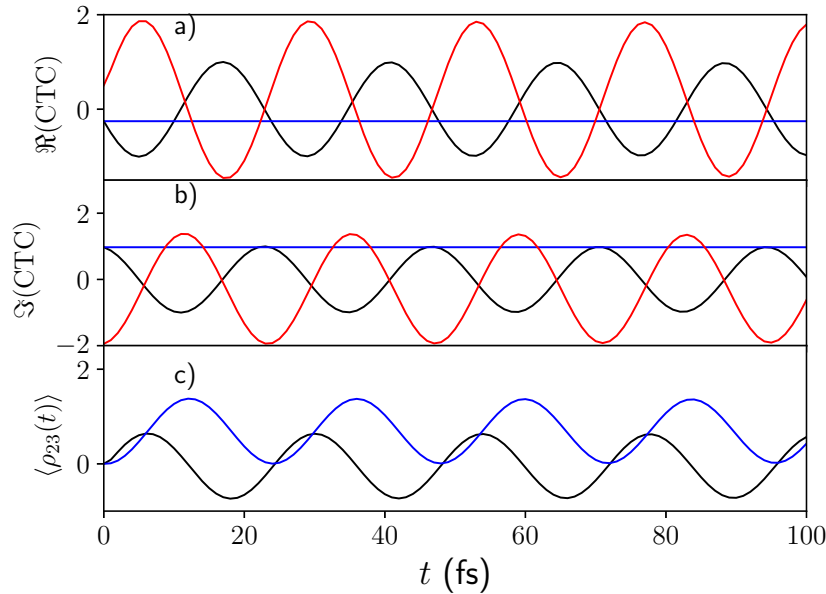

Figure 6: a) Real CTCs; black, blue and red colors are for the first, second and third element in parenthesis respectively; b) imaginary CTCs; c) real (black) and imaginary (blue) part of $\rho^e_{23}(t)$ at $\nu = 0$.

Coherences $\rho^e_{\beta\alpha}(t)$ ($\beta \neq \alpha$), on the other hand, are well behaved in the limit $\nu \to 0$. This can immediately be seen if we rewrite Eq. (51) in the equivalent form (cf. Ref. [16]):

$$G^a_{\beta\alpha}(\omega) = \frac{\sigma^a_{\beta\alpha}}{2\nu + i\omega_{\beta\alpha}} \left[\frac{1}{\nu - i(\omega - \omega_{\beta a})} + \frac{1}{\nu + i(\omega - \omega_{\alpha a})} \right]. \tag{32}$$

Then ν can safely be set to zero in the first term (since $\omega_{\beta\alpha} \neq 0$), while the real and imaginary parts of the two terms in the square brackets produce, correspondingly, delta-function and the principal value contribution. Unfortunately, the latter cannot be evaluated analytically in Eq. (28). Yet the numerical evaluation confirms that all integrals exist in the limit $\nu \to 0$. For illustration, we calculated coherences $\rho^e_{23}(t)$ for the three-level system with $\varepsilon_2 = 1.5\,\text{eV} = 12097\,\text{cm}^{-1}$, $\varepsilon_3 = \varepsilon_2 + \Omega$, $e_1 = 0$, and thermal field at 6000 K. The left and middle panels of figure 6 display, correspondingly, the real and imaginary part of the three CTCs of the density matrix $\rho^e_{23}(t)$, as defined in Eq. (29). The first and third CTCs exhibit undamped oscillations with the vibrational period of $2\pi/\Omega = 24$ fs, while the second CTC is constant. The right panel of figure 6 shows the real and and imaginary part of $\rho^e_{23}(t)$ which correspond to the sum of three CTCs in the left and middle panels, respectively. They are described by the characteristic periodic functions, which are up-shifted and phase-shifted with respect to each other (cf. Ref. [94]).

According to Eq. (32), the ratio of the absolute values of populations and coherences of the density matrix can be estimated as

$$\left| \frac{\rho^e_{\alpha\alpha}(t)}{\rho^e_{\beta\alpha}(t)} \right| \approx \sqrt{1 + \frac{\omega^2_{\beta\alpha}}{4\nu^2}}. \tag{33}$$

Hence if the inverse of the excited state lifetime ν is comparable with characteristic energy spacing of the system $\omega_{\beta\alpha}$, then populations and coherences are of the same order of magnitude. If, however, $\nu \ll \omega_{\beta\alpha}$, then populations are orders of magnitude larger than coherences. Realistically, $\omega_{\beta\alpha}$ are of the order $\sim 100 - 1000$ cm^{-1} or vibrational periods $2\pi/\omega_{\beta\alpha}$ are of the order $\sim 10 - 100$ fs. The comparable ν may occur in molecular systems experiencing

fast excited-state depopulation, for example via conical intersection. In the limit of radiative lifetime corresponding to ν^{-1} of several nanoseconds, populations will be several orders of magnitude higher than coherences. If $\nu = 0$, as in the simulations of the present work, then second-order perturbation theory breaks down $(\rho_{\alpha\alpha}^e(t) \sim t)$ and nonperturbative treatment of the system-field interaction is necessary.

This simple analysis shows that, in general, instantaneously switched-on thermal radiation creates coherent density matrix $\rho_{\beta\alpha}^e(t)$, as was emphasized by Brumer and coworkers.[8,9] Therefore, expectation value of any operator $\mathcal{O}$, $\langle\mathcal{O}\rho^e(t)\rangle$, will exhibit oscillations provided some of the off-diagonal matrix elements of this operator are nonzero, $\mathcal{O}_{\beta\alpha} \neq 0$. This is fully corroborated by the numerically exact simulations of the present work. However, the ratio of incoherent and coherent contributions to $\langle\mathcal{O}\rho^e(t)\rangle$ is regulated by Eq. (33).

Note, finally, that the density matrix induced by the instantaneous coherent laser pulse reads

$$\rho_{\beta\alpha}^e(t) = \sigma_{\beta\alpha} e^{-(2\nu + i\omega_{\beta\alpha})t} \tag{34}$$

where $\sigma_{\beta\alpha}$ is given by Eq. (47). Obviously, this expression is quite similar to the contribution to the density matrix of Eq. (28) due to the first term in the parenthesis in Eq. (29). However, the density matrix of Eq. (28) possesses, additionally, a stationary contribution due to the second term in the parenthesis in Eq. (29). This stationary contribution can be considered as a signature of thermal light.[30]

5   Conclusions

We have developed a new methodology based on the TFD-TT theory that can be used to describe a system interacting with two thermal baths at different temperatures. The methodology permits numerically accurate simulations of the quantum dynamics of an electronic/excitonic system coupled to nuclear and photonic baths described by arbitrary spectral densities and for any system-bath coupling strengths. The methodology has been used to

describe the evolution of a molecular system interacting with thermal radiation bath at 6000 K mimicking the effect of sunlight. As molecular systems, we considered a single-vibrational-mode molecule and a vibronic dimer thermalized at 300 K. The TFD Schrödinger equation has then been solved using a recently developed time-adaptive and bond-adaptive algorithm based on the TT description of the molecular wave-function.

Our numerically accurate simulations show that an instantaneously switched-on thermal light source can generate a coherent superposition of molecular states, which is destroyed on a much longer timescale than the typical coherence time of a thermal radiation. This behaviour is independent of the complexity of the system, as also confirmed by the model dimer calculation, and depends solely on the pattern of the eigenenergies of the system. Similar results were demonstrated earlier on several model systems by applying approximate methods of the description of the system-field interaction. We point out that the persistence of the oscillations in more realistic systems might be compromised by other dissipative mechanisms, however this is irrelevant for our results which aim at clarifying by numerically exact methods the role of the thermal radiation field and not of the complexity of the molecular system under examination. In future work we will extend our model to more complex cases by studying the role of the incoherent excitation process on the exciton transfer dynamics in large molecular aggregates as well as explore molecular systems in microcavities, in which system-field interaction can vary from weak to strong system-field coupling regimes.

Finally, the paper also shows that the tAMEn time and bond adaptive time-integration of the TFD-TT equations is extremely useful when accurate and converged results are required for relatively long propagation times.[54]

Acknowledgement

6   Appendix

The system Hamiltonian H_S of Eq. (12) commutes with the excitonic number operator $N = \sum_n c_n^\dagger c_n$ ($[H_S, N] = 0$), and we can therefore classify H_S according to the expectation value $\langle N \rangle$. Retaining only the ground state g ($\langle N \rangle = 0$) and the singly-excited state e ($\langle N \rangle = 1$) we can write the system Hamiltonian as $H_S = H_g + H_e$. In the eigenfunction representation,

$$H_g = \sum_a e_a |a\rangle\langle a|, \quad H_e = \sum_\alpha \varepsilon_\alpha |\alpha\rangle\langle\alpha|. \tag{35}$$

and transition frequencies read

$$\omega_{\alpha a} = \varepsilon_\alpha - e_a, \quad \omega_{\alpha\beta} = \varepsilon_\alpha - \varepsilon_\beta. \tag{36}$$

Hereafter, Latin (Greek) dummy indexes label eigenvalues and eigenfunctions of H_g (H_e). The system-bath interaction Hamiltonian of Eq. (3) then assumes the form

$$H_{SB} = V \sum_{a\alpha} \mu_{a\alpha} \left(|a\rangle\langle\alpha| + |\alpha\rangle\langle a| \right) \tag{37}$$

where $\mu_{a\alpha}$ are the matrix elements of the transition dipole moment operators.

Since we adopt the eigenfunction representation of the system Hamiltonian, it is more convenient to work with the Liouville equation

$$\partial_t \rho(t) = -i[H, \rho(t)] \tag{38}$$

which has to be solved with the factorized initial condition

$$\rho(0) = \rho_S \rho_B \tag{39}$$

where

$$\rho_S = Z_S^{-1} \sum_a |a\rangle\langle a| e^{-\beta_1 e_a}, \tag{40}$$

$$\rho_B = Z_B^{-1} e^{-\beta_2 H_B}, \tag{41}$$

and Z_S, Z_B are the partitioned functions. We thus assume that the system-bath interaction is switched on at $t = 0$.

Changing to the interaction representation (subscript I) with respect to $H_S + H_B$, we obtain:

$$\partial_t \rho_I(t) = i[H_I(t), \rho_I(t)], \tag{42}$$

where

$$H_I(t) = e^{i(H_S + H_B)t} H_{SB} e^{-i(H_S + H_B)t} = V(t) \sum_{a\alpha} \mu_{a\alpha} \left(e^{-i\omega_{\alpha a} t} |b\rangle\langle\alpha| + e^{i\omega_{\alpha a} t} |\alpha\rangle\langle a| \right) \tag{43}$$

and

$$V(t) = \sum_k \gamma_k (b_k^\dagger e^{i\omega_k t} + b_k e^{-i\omega_k t}). \tag{44}$$

In second-order perturbation theory, the excited-state density matrix is determined as

$$\rho_I^e(t) = \mathrm{Tr}_B \left\{ \int_0^t dt' \int_0^{t'} dt'' \, H_I(t') \rho_I(0) H_I(t'') + H.c. \right\}. \tag{45}$$

Taking trace with respect to the photon degrees of freedom we obtain (cf. Refs. [8,9])

$$\rho_I^e(t) = \sum_{a\alpha\beta} \sigma_{\alpha\beta}^a \int_0^t dt' \int_0^{t'} dt'' C^{BB}(t'' - t') e^{\nu(t'+t'')} e^{i\omega_{\beta a} t'} e^{-i\omega_{\alpha a} t''} |\beta\rangle\langle\alpha| \rho_B + H.c. \tag{46}$$

29

where $C^{BB}(t)$ is the correlation function of the electric field defined per Eq. (5) and

$$\sigma_{\alpha\beta}^a = \mu_{a\alpha}\mu_{a\beta}Z_S^{-1}e^{-\beta_1\varepsilon_a}. \tag{47}$$

To make the time integrals in Eq. (46) convergent, we introduced the excited-state lifetime ν^{-1} (that is, replaced $\varepsilon_\alpha \to \varepsilon_\alpha - i\nu$). This procedure can be considered as regularization of the integrals, notably if the limit $\nu \to 0$ can be taken in the final expressions.

Changing variables according to $t' - t'' = \tau$ and integrating by parts, we obtain:

$$\rho_I^e(t) = \sum_{a\alpha\beta} \sigma_{\alpha\beta}^a \frac{1}{-2\nu - i\omega_{\beta\alpha}} \int_0^t d\tau C^{BB}(-\tau)e^{\nu\tau}e^{i\omega_{\beta a}\tau}\left\{1 - e^{(2\nu + i\omega_{\beta\alpha})(t-\tau)}\right\}|\beta\rangle\langle\alpha| + H.c. \tag{48}$$

Expressing $C^{BB}(t)$ through the spectral density $J(\omega)$ of Eq. (8) and integrating over τ we obtain

$$\rho_I^e(t) = \sum_{\alpha\beta;a} \int d\omega J(\omega) \left(\overline{G}_{\beta\alpha}^a(\omega,t)n(\omega) + \overline{G}_{\beta\alpha}^a(-\omega,t)(1 + n(\omega))\right)|\beta\rangle\langle\alpha|. \tag{49}$$

Here

$$\overline{G}_{\beta\alpha}^a(\omega,t) = G_{\beta\alpha}^a(\omega)\left(1 + e^{2\nu t}e^{i\omega_{\beta\alpha}t} - e^{\nu t}\left[e^{-i(\omega - \omega_{\beta a})t} + e^{i(\omega - \omega_{\alpha a})t}\right]\right), \tag{50}$$

$$G_{\beta\alpha}^a(\omega) = \frac{\sigma_{\beta\alpha}^a}{[\nu - i(\omega - \omega_{\beta a})][\nu + i(\omega - \omega_{\alpha a})]}. \tag{51}$$

Returning back to the original representation, we get

$$\rho^e(t) = \sum_{\alpha\beta} \rho_{\beta\alpha}^e(t)|\beta\rangle\langle\alpha|, \tag{52}$$

$$\rho_{\beta\alpha}^e(t) = \sum_a \int d\omega J(\omega)\left(G_{\beta\alpha}^a(\omega,t)n(\omega) + G_{\beta\alpha}^a(-\omega,t)(1 + n(\omega))\right) \tag{53}$$

where

$$G_{\beta\alpha}^a = \overline{G}_{\beta\alpha}^a(\omega,t)e^{-(2\nu + i\omega_{\beta\alpha})t} \tag{54}$$

is explicitly defined by Eq. (29). Finally, since typical values of $\omega_{\beta a}$ in molecular and

excitonic systems correspond to several eV, we can apply the rotating wave approximation, retain only resonant contributions, neglect off-resonant terms proportional to $G^a_{\beta\alpha}(-\omega, t)$ and obtain Eq. (28). In this case, regularization of $J(\omega)$ is not necessary, we can take $J(\omega) = \omega^3$, and then $J(\omega)n(\omega)$ is nothing but Plank's function.

References

(1) Hestand, N. J.; Spano, F. C. Expanded Theory of H- and J-Molecular Aggregates: The Effects of Vibronic Coupling and Intermolecular Charge Transfer. *Chem. Rev.* **2018**, *118*, 7069–7163.

(2) Spano, F. C. Excitons in Conjugated Oligomer Aggregates, Films, and Crystals. *Annu. Rev. Phys. Chem.* **2006**, *57*, 217–243.

(3) Panhans, M.; Hutsch, S.; Benduhn, J.; Schellhammer, K. S.; Nikolis, V. C.; Vangerven, T.; Vandewal, K.; Ortmann, F. Molecular Vibrations Reduce the Maximum Achievable Photovoltage in Organic Solar Cells. *Nat. Commun.* **2020**, *11*, 1488.

(4) Mukamel, S. *Principles of Nonlinear Optical Spectroscopy.*; Oxford University Press: Oxford, 1999.

(5) Gelin, M. F.; Chen, L.; Domcke, W. Equation-of-Motion Methods for the Calculation of Femtosecond Time-Resolved 4-Wave-Mixing and N-Wave-Mixing Signals. *Chem. Rev.* **2022**, *122*, 17339–17396.

(6) Cho, M.; Fleming, G. R. In *Advances in Chemical Physics*; Prigogine, I., Rice, S. A., Eds.; John Wiley & Sons, Inc.: Hoboken, NJ, USA, 2007; pp 311–370.

(7) Thyrhaug, E.; Tempelaar, R.; Alcocer, M. J. P.; Žídek, K.; Bína, D.; Knoester, J.; Jansen, T. L. C.; Zigmantas, D. Identification and Characterization of Diverse Coherences in the Fenna–Matthews–Olson Complex. *Nat. Chem.* **2018**, *10*, 780.

(8) Jiang, X.-P.; Brumer, P. Creation and Dynamics of Molecular States Prepared with Coherent vs Partially Coherent Pulsed Light. *J. Chem. Phys.* **1991**, *94*, 5833–5843.

(9) Brumer, P. Shedding (Incoherent) Light on Quantum Effects in Light-Induced Biological Processes. *J. Phys. Chem. Lett.* **2018**, *9*, 2946–2955.

(10) Brumer, P.; Shapiro, M. Molecular Response in One-Photon Absorption via Natural Thermal Light vs. Pulsed Laser Excitation. *Proc. Natl. Acad. Sci.* **2012**, *109*, 19575–19578.

(11) Scholes, G. D.; Fleming, G. R.; Chen, L. X.; Aspuru-Guzik, A.; Buchleitner, A.; Coker, D. F.; Engel, G. S.; van Grondelle, R.; Ishizaki, A.; Jonas, D. M.; Lundeen, J. S.; McCusker, J. K.; Mukamel, S.; Ogilvie, J. P.; Olaya-Castro, A.; Ratner, M. A.; Spano, F. C.; Whaley, K. B.; Zhu, X. Using Coherence to Enhance Function in Chemical and Biophysical Systems. *Nature* **2017**, *543*, 647–656.

(12) Mukamel, S. Comment on "Coherence and Uncertainty in Nanostructured Organic Photovoltaics". *J. Phys. Chem. A* **2013**, *117*, 10563–10564.

(13) Pachón, L. A.; Brumer, P. Incoherent Excitation of Thermally Equilibrated Open Quantum Systems. *Phys. Rev. A* **2013**, *87*, 022106.

(14) Avisar, D.; Wilson-Gordon, A. D. Thermal-Light-Induced Dynamics: Coherence and Revivals in V-Type and Molecular Jaynes-Cummings Systems. *Phys. Rev. A* **2016**, *93*, 033843.

(15) Dodin, A.; Tscherbul, T. V.; Brumer, P. Quantum Dynamics of Incoherently Driven V-type Systems: Analytic Solutions beyond the Secular Approximation. *The Journal of Chemical Physics* **2016**, *144*, 244108.

(16) Mančal, T.; Valkunas, L. Exciton Dynamics in Photosynthetic Complexes: Excitation by Coherent and Incoherent Light. *New J. Phys.* **2010**, *12*, 065044.

(17) Chenu, A.; Brumer, P. Transform-Limited-Pulse Representation of Excitation with Natural Incoherent Light. *J. Chem. Phys.* **2016**, *144*.

(18) Van Kampen, N. G. The Case against Linear Response Theory. *Phys. Norveg.* **1971**, *5*, 279.

(19) Van Vliet, C. M. On van Kampen's Objections against Linear Response Theory. *J Stat Phys* **1988**, *53*, 49–60.

(20) Kryvohuz, M.; Cao, J. Classical Divergence of Nonlinear Response Functions. *Phys. Rev. Lett.* **2006**, *96*, 030403.

(21) Malinin, S. V.; Chernyak, V. Y. Classical Nonlinear Response of a Chaotic System. I. Collective Resonances. *Phys. Rev. E* **2008**, *77*, 056201.

(22) Reppert, M.; Brumer, P. Classical Coherent Two-Dimensional Vibrational Spectroscopy. *The Journal of Chemical Physics* **2018**, *148*, 064101.

(23) Gardiner, C.; Zoller, P. *Quantum Noise: A Handbook of Markovian and Non-Markovian Quantum Stochastic Methods with Applications to Quantum Optics*; Springer Science & Business Media, 2004.

(24) Breuer, H.-P.; Petruccione, F. *The Theory of Open Quantum Systems*; Oxford University Press: Oxford [England]; New York, 2010.

(25) Shatokhin, V. N.; Walschaers, M.; Schlawin, F.; Buchleitner, A. Coherence Turned on by Incoherent Light. *New J. Phys.* **2018**, *20*, 113040.

(26) Bourne Worster, S.; Stross, C.; Vaughan, F. M. W. C.; Linden, N.; Manby, F. R. Structure and Efficiency in Bacterial Photosynthetic Light Harvesting. *J. Phys. Chem. Lett.* **2019**, *10*, 7383–7390.

(27) Dodin, A.; Tscherbul, T. V.; Brumer, P. Coherent Dynamics of V-type Systems Driven by Time-Dependent Incoherent Radiation. *The Journal of Chemical Physics* **2016**, *145*, 244313.

(28) Dodin, A.; Tscherbul, T.; Alicki, R.; Vutha, A.; Brumer, P. Secular versus Nonsecular Redfield Dynamics and Fano Coherences in Incoherent Excitation: An Experimental Proposal. *Phys. Rev. A* **2018**, *97*, 013421.

(29) Tscherbul, T. V.; Brumer, P. Partial Secular Bloch-Redfield Master Equation for Incoherent Excitation of Multilevel Quantum Systems. *J. Chem. Phys.* **2015**, *142*, 104107.

(30) Pachón, L. A.; Botero, J. D.; Brumer, P. Open System Perspective on Incoherent Excitation of Light-Harvesting Systems. *J. Phys. B: At. Mol. Opt. Phys.* **2017**, *50*, 184003.

(31) Calderón, L. F.; Pachón, L. A. Nonadiabatic Sunlight Harvesting. *Phys. Chem. Chem. Phys.* **2020**, *22*, 12678–12687.

(32) Dijkstra, A. G.; Tanimura, Y. The Role of the Environment Time Scale in Light-Harvesting Efficiency and Coherent Oscillations. *New J. Phys.* **2012**, *14*, 073027.

(33) Kreisbeck, C.; Kramer, T. Long-Lived Electronic Coherence in Dissipative Exciton Dynamics of Light-Harvesting Complexes. *J. Phys. Chem. Lett.* **2012**, *3*, 2828–2833.

(34) Fassioli, F.; Olaya-Castro, A.; Scholes, G. D. Coherent Energy Transfer under Incoherent Light Conditions. *J. Phys. Chem. Lett.* **2012**, *3*, 3136–3142.

(35) Maguire, H.; Iles-Smith, J.; Nazir, A. Environmental Nonadditivity and Franck-Condon Physics in Nonequilibrium Quantum Systems. *Phys. Rev. Lett.* **2019**, *123*, 093601.

(36) Mitchison, M. T.; Plenio, M. B. Non-Additive Dissipation in Open Quantum Networks out of Equilibrium. *New J. Phys.* **2018**, *20*, 033005.

(37) Olšina, J.; Dijkstra, A. G.; Wang, C.; Cao, J. Can Natural Sunlight Induce Coherent Exciton Dynamics? 2014.

(38) Janković, V.; Mančal, T. Exact Description of Excitonic Dynamics in Molecular Aggregates Weakly Driven by Light. *J. Chem. Phys.* **2020**, *153*, 244122.

(39) Janković, V.; Mančal, T. Nonequilibrium Steady-State Picture of Incoherent Light-Induced Excitation Harvesting. *J. Chem. Phys.* **2020**, *153*, 244110.

(40) Ko, L.; Cook, R. L.; Whaley, K. B. Dynamics of Photosynthetic Light Harvesting Systems Interacting with N-photon Fock States. *J. Chem. Phys.* **2022**, *156*, 244108.

(41) Barbatti, M. Simulation of Excitation by Sunlight in Mixed Quantum-Classical Dynamics. *J. Chem. Theory Comput.* **2020**, *16*, 4849–4856.

(42) Wang, H.; Thoss, M. Multilayer Formulation of the Multiconfiguration Time-Dependent Hartree Theory. *J. Chem. Phys.* **2003**, *119*, 1289–1299.

(43) Manthe, U. A Multilayer Multiconfigurational Time-Dependent Hartree Approach for Quantum Dynamics on General Potential Energy Surfaces. *J. Chem. Phys.* **2008**, *128*, 164116–14.

(44) Borrelli, R.; Gelin, M. F. Quantum Electron-Vibrational Dynamics at Finite Temperature: Thermo Field Dynamics Approach. *J. Chem. Phys.* **2016**, *145*, 224101.

(45) Borrelli, R. Theoretical Study of Charge-Transfer Processes at Finite Temperature Using a Novel Thermal Schrödinger Equation. *Chemical Physics* **2018**, *515*, 236–241.

(46) Borrelli, R.; Gelin, M. F. Finite Temperature Quantum Dynamics of Complex Systems: Integrating Thermo-Field Theories and Tensor-Train Methods. *WIREs Comput. Mol. Sci.* **2021**, *11*, e1539.

(47) Borrelli, R. Density Matrix Dynamics in Twin-Formulation: An Efficient Methodology Based on Tensor-Train Representation of Reduced Equations of Motion. *J. Chem. Phys.* **2019**, *150*, 234102.

(48) Gelin, M. F.; Velardo, A.; Borrelli, R. Efficient Quantum Dynamics Simulations of Complex Molecular Systems: A Unified Treatment of Dynamic and Static Disorder. *J. Chem. Phys.* **2021**, *155*, 134102.

(49) Chin, A. W.; Prior, J.; Rosenbach, R.; Caycedo-Soler, F.; Huelga, S. F.; Plenio, M. B. The Role of Non-Equilibrium Vibrational Structures in Electronic Coherence and Recoherence in Pigment-Protein Complexes. *Nat Phys* **2013**, *9*, 113–118.

(50) Tamascelli, D.; Smirne, A.; Lim, J.; Huelga, S. F.; Plenio, M. B. Efficient Simulation of Finite-Temperature Open Quantum Systems. *Phys. Rev. Lett.* **2019**, *123*, 090402.

(51) del Pino, J.; Schröder, F. A. Y. N.; Chin, A. W.; Feist, J.; Garcia-Vidal, F. J. Tensor Network Simulation of Non-Markovian Dynamics in Organic Polaritons. *Phys. Rev. Lett.* **2018**, *121*, 227401.

(52) Bulla, R.; Tong, N.-H.; Vojta, M. Numerical Renormalization Group for Bosonic Systems and Application to the Sub-Ohmic Spin-Boson Model. *Phys. Rev. Lett.* **2003**, *91*, 170601.

(53) Dolgov, S. V. A Tensor Decomposition Algorithm for Large ODEs with Conservation Laws. *Comput. Methods Appl. Math.* **2019**, *19*, 23–38.

(54) Borrelli, R.; Dolgov, S. Expanding the Range of Hierarchical Equations of Motion by Tensor-Train Implementation. *J. Phys. Chem. B* **2021**, *125*, 5397–5407.

(55) Messiah, A. *Quantum Mechanics*; Wiley, New York, 1962.

(56) Feynman, R. P.; Vernon, F. L. The Theory of a General Quantum System Interacting with a Linear Dissipative System. *Ann. Phys.* **1963**, *24*, 118–173.

(57) Pachón, L. A.; Brumer, P. Quantum Driven Dissipative Parametric Oscillator in a Blackbody Radiation Field. *J. Math. Phys.* **2014**, *55*, 012103.

(58) Tanimura, Y. Stochastic Liouville, Langevin, Fokker–Planck, and Master Equation Approaches to Quantum Dissipative Systems. *J. Phys. Soc. Jpn.* **2006**, *75*, 082001.

(59) Kano, Y.; Wolf, E. Temporal Coherence of Black Body Radiation. *Proc. Phys. Soc.* **1962**, *80*, 1273–1276.

(60) Mehta, C. L. Coherence-Time and Effective Bandwidth of Blackbody Radiation. *Nuovo Cim* **1963**, *28*, 401–408.

(61) Bourret, R. C. Coherence Properties of Blackbody Radiation. *Nuovo Cim* **1960**, *18*, 347–356.

(62) Wang, H.; Thoss, M.; Sorge, K. L.; Gelabert, R.; Giménez, X.; Miller, W. H. Semi-classical Description of Quantum Coherence Effects and Their Quenching: A Forward–Backward Initial Value Representation Study. *J. Chem. Phys.* **2001**, *114*, 2562–2571.

(63) Sim, E.; Makri, N. Path Integral Simulation of Charge Transfer Dynamics in Photosynthetic Reaction Centers. *J. Phys. Chem. B* **1997**, *101*, 5446–5458.

(64) Gelin Maxim F.,; Borrelli Raffaele, Thermal Schrödinger Equation: Efficient Tool for Simulation of Many-Body Quantum Dynamics at Finite Temperature. *Annalen der Physik* **2017**, *529*, 1700200.

(65) Takahashi, Y.; Umezawa, H. Thermo Field Dynamics. *Int. J. Mod. Phys. B* **1996**, *10*, 1755–1805.

(66) Grinev, T.; Brumer, P. Realistic vs Sudden Turn-on of Natural Incoherent Light: Coherences and Dynamics in Molecular Excitation and Internal Conversion. *The Journal of Chemical Physics* **2015**, *143*, 244313.

(67) Oseledets, I.; Tyrtyshnikov, E. Breaking the Curse of Dimensionality, Or How to Use SVD in Many Dimensions. *SIAM J. Sci. Comput.* **2009**, *31*, 3744–3759.

(68) Wang, H. Multilayer Multiconfiguration Time-Dependent Hartree Theory. *J. Phys. Chem. A* **2015**, *119*, 7951–7965.

(69) Zhao, Y. The Hierarchy of Davydov's Ansätze: From Guesswork to Numerically "Exact" Many-Body Wave Functions. *The Journal of Chemical Physics* **2023**, *158*, 080901.

(70) Tanimura, Y. Numerically "Exact" Approach to Open Quantum Dynamics: The Hierarchical Equations of Motion (HEOM). *J. Chem. Phys.* **2020**, *153*, 020901.

(71) Makri, N.; Makarov, D. E. Tensor Propagator for Iterative Quantum Time Evolution of Reduced Density Matrices. I. Theory. *J. Chem. Phys.* **1995**, *102*, 4600–4610.

(72) Bachmayr, M.; Schneider, R.; Uschmajew, A. Tensor Networks and Hierarchical Tensors for the Solution of High-Dimensional Partial Differential Equations. *Found Comput Math* **2016**, *16*, 1423–1472.

(73) Lubich, C.; Rohwedder, T.; Schneider, R.; Vandereycken, B. Dynamical Approximation by Hierarchical Tucker and Tensor-Train Tensors. *SIAM. J. Matrix Anal. & Appl.* **2013**, *34*, 470–494.

(74) Oseledets, I. Tensor-Train Decomposition. *SIAM J. Sci. Comput.* **2011**, *33*, 2295–2317.

(75) Lubich, C.; Oseledets, I.; Vandereycken, B. Time Integration of Tensor Trains. *SIAM J. Numer. Anal.* **2015**, *53*, 917–941.

(76) Holtz, S.; Rohwedder, T.; Schneider, R. On Manifolds of Tensors of Fixed TT-rank. *Numer. Math.* **2011**, *120*, 701–731.

(77) Vidal, G. Efficient Simulation of One-Dimensional Quantum Many-Body Systems. *Phys. Rev. Lett.* **2004**, *93*, 040502.

(78) Wall, M. L.; Carr, L. D. Out-of-Equilibrium Dynamics with Matrix Product States. *New J. Phys.* **2012**, *14*, 125015.

(79) García-Ripoll, J. J. Time Evolution of Matrix Product States. *New J. Phys.* **2006**, *8*, 305.

(80) Haegeman, J.; Lubich, C.; Oseledets, I.; Vandereycken, B.; Verstraete, F. Unifying Time Evolution and Optimization with Matrix Product States. *Phys. Rev. B* **2016**, *94*, 165116.

(81) Greene, S. M.; Batista, V. S. Tensor-Train Split-Operator Fourier Transform (TT-SOFT) Method: Multidimensional Nonadiabatic Quantum Dynamics. *J. Chem. Theory Comput.* **2017**, *13*, 4034–4042.

(82) Soley, M. B.; Bergold, P.; Gorodetsky, A. A.; Batista, V. S. Functional Tensor-Train Chebyshev Method for Multidimensional Quantum Dynamics Simulations. *J. Chem. Theory Comput.* **2021**,

(83) Yan, Y.; Xing, T.; Shi, Q. A New Method to Improve the Numerical Stability of the Hierarchical Equations of Motion for Discrete Harmonic Oscillator Modes. *J. Chem. Phys.* **2020**, *153*, 204109.

(84) Trefethen, L. N. *Spectral Methods in MATLAB*; Society for Industrial and Applied Mathematics, 2000.

(85) Dolgov, S.; Savostyanov, D. Alternating Minimal Energy Methods for Linear Systems in Higher Dimensions. *SIAM J. Sci. Comput.* **2014**, *36*, A2248–A2271.

(86) Holtz, S.; Rohwedder, T.; Schneider, R. The Alternating Linear Scheme for Tensor Optimization in the Tensor Train Format. *SIAM J. Sci. Comput.* **2012**, *34*, A683–A713.

(87) Borrelli, R.; Domcke, W. First-Principles Study of Photoinduced Electron-Transfer Dynamics in a Mg–Porphyrin–Quinone Complex. *Chem. Phys. Lett.* **2010**, *498*, 230–234.

(88) Borrelli, R.; Ellena, S.; Barolo, C. Theoretical and Experimental Determination of the Absorption and Emission Spectra of a Prototypical Indolenine-Based Squaraine Dye. *Phys. Chem. Chem. Phys.* **2014**, *16*, 2390–2398.

(89) Koyu, S.; Dodin, A.; Brumer, P.; Tscherbul, T. V. Steady-State Fano Coherences in a V-type System Driven by Polarized Incoherent Light. *Phys. Rev. Res.* **2021**, *3*, 013295.

(90) Naim, W.; Novelli, V.; Nikolinakos, I.; Barbero, N.; Dzeba, I.; Grifoni, F.; Ren, Y.; Alnasser, T.; Velardo, A.; Borrelli, R.; Haacke, S.; Zakeeruddin, S. M.; Graetzel, M.; Barolo, C.; Sauvage, F. Transparent and Colorless Dye-Sensitized Solar Cells Exceeding 75% Average Visible Transmittance. *JACS Au* **2021**, *1*, 409–426.

(91) Grifoni, F.; Bonomo, M.; Naim, W.; Barbero, N.; Alnasser, T.; Dzeba, I.; Giordano, M.; Tsaturyan, A.; Urbani, M.; Torres, T.; Barolo, C.; Sauvage, F. Toward Sustainable, Colorless, and Transparent Photovoltaics: State of the Art and Perspectives for the Development of Selective Near-Infrared Dye-Sensitized Solar Cells. *Adv. Energy Mater.* **2021**, *11*, 2101598.

(92) Sung, J.; Kim, P.; Fimmel, B.; Würthner, F.; Kim, D. Direct Observation of Ultrafast Coherent Exciton Dynamics in Helical π-Stacks of Self-Assembled Perylene Bisimides. *Nat. Commun.* **2015**, *6*, 8646.

(93) Cainelli, M.; Borrelli, R.; Tanimura, Y. Effect of Mixed Frenkel and Charge Transfer States in Time-Gated Fluorescence Spectra of Perylene Bisimides H-aggregates: Hierarchical Equations of Motion Approach. *J. Chem. Phys.* **2022**,

(94) Sadeq, Z. S.; Brumer, P. Transient Quantum Coherent Response to a Partially Coherent Radiation Field. *J. Chem. Phys.* **2014**, *140*, 074104.

TOC Graphic

$$\langle g|$$
$$\otimes$$
$$(\omega_i b_i^\dagger b_i)$$
$$\otimes$$
$$|e_1\rangle, |e_2\rangle, ...$$

?

$$\{p_1 |e_1\rangle, p_2 |e_2\rangle, ...\}$$
incoherent

coherent
$$c_1 |e_1\rangle + c_2 |e_2\rangle + ...$$